PAPER

Check for updates

Fabrication of patterned calcium carbonate materials through template-assisted microbially induced calcium carbonate precipitation†

Dewei Yi,‡[ab] Hong Zhang,‡[ab] Wenchao Zhang,[c] Yiwu Zong [ID][ab] and Kun Zhao [ID] *[ab]

Patterned calcium carbonate materials with controlled morphologies have broad applications in both environmental and engineering fields. However, how to fabricate such materials through environmental-friendly methods under ambient conditions is still challenging. Here, we report a green approach for fabricating patterned calcium carbonate materials. This eco-friendly approach is based on template-assisted microbially induced calcium carbonate precipitation. As a proof of concept, by varying the templates and optimizing fabrication parameters, different patterned calcium carbonate materials were obtained. The optimized parameters include $C_{Ca^{2+}} = 80$ mM, $T_i = 15$ °C, and templates made of small-sized $CaCO_3$ particles with a concentration of 1.5 mg mL^{-1}, under which better and more sharp patterns were obtained. Materials with periodic patterns were also fabricated through a periodic template, showing good scalability of this approach. The results of this study could mean great potential in applications where spatially controlled calcium carbonate depositions with user-designed patterns are needed.

Introduction

Calcium carbonate is one of the most abundant biominerals in nature,[1] and has broad technological applications, for example, as coating materials in fabricating light-weight ceramics and catalysis support materials,[2] as well as bone-regeneration materials for biomedical implants.[3] For such applications, the techniques to deposit directly the patterned calcium carbonate films with controlled morphologies through environmental-friendly methods under ambient conditions are ideal and in high demand.

For chemical synthesis of patterned calcium carbonate materials, techniques based on templated organic surfaces such as Langmuir monolayers,[4–6] self-assembled monolayers (SAMs)[7–11] and polyelectrolyte multilayer film[12] *etc.*, have been developed. Particularly, the SAM method has been shown to be able to form ordered ceramic films with a high spatial resolution and controllable crystal morphologies.[8–11] Compared with such chemical synthesis methods, techniques based on

microbially induced calcium carbonate precipitation (MICP)[13,14] are green and eco-friendly, and they are performed under ambient conditions. Thus, fabrication of calcium carbonate through MICP techniques is a promising way to meet the increasingly high requirement of aforementioned applications.

MICP is a common phenomenon in nature observed in a variety of microorganisms including the urease producer bacterium – *Sporosarcina pasteurii* (*S. pasteurii*),[15–18] which can be performed by ureolysis[19] or by denitrification.[20] Ureolytic MICP[13] is one of the widely used environmental-friendly bio-mineralization techniques due to its simple hydrolysis mechanism and high reaction activity. Many studies on MICP have been focused on polymorphs of precipitated calcium carbonates and the dependence of MICP activities on environmental factors such as pH, temperature, and calcium concentrations *etc.*[21–28] However, compared with the aforementioned abundant reports on chemically synthesis of patterned calcium carbonate materials, there has been no study, to the best of our knowledge, reported on the fine spatial control of calcium carbonate precipitation during MICP, which is the key for applying MICP techniques into the fabrication of patterned calcium carbonate materials.

In an earlier work,[29] Zhang *et al.* observed that $CaCO_3$ particles obtained from precipitation in previous MICP runs can act as nucleating sites to support the growth of newly precipitated calcium carbonate in fresh MICP runs. Inspired by this observation, in this work, we reported an approach for the fabrication of patterned calcium carbonate materials using the MICP technique *via* heterogenous template-promoted

[a]Frontier Science Center for Synthetic Biology, Key Laboratory of Systems Bioengineering (Ministry of Education), Tianjin University, Tianjin 300072, P. R. China. E-mail: kunzhao@tju.edu.cn

[b]School of Chemical Engineering and Technology, Tianjin University, Tianjin 300072, P. R. China

[c]School of Chemistry and Life Science, Suzhou University of Science and Technology, Suzhou 215009, P. R. China

† Electronic supplementary information (ESI) available. See DOI: 10.1039/d1ra04072c

‡ These authors contributed equally in this work.

precipitation. The aim of this study is to show whether and how $CaCO_3$ particles can be used to pattern MICP precipitations. The templates were formed by $CaCO_3$ particles obtained from MICP precipitates, which resulted in a promoted growth of calcium carbonate on templated regions when they were immersed in MICP cultures. Such promoted growth finally led to patterned calcium carbonate materials whose spatial distribution on the substrate is governed by the template patterns. The MICP process was also optimized by tuning environmental factors such as the concentration and size of $CaCO_3$ particles used for making templates, Ca^{2+} concentration and cultural temperature.

Results

Fabrication of patterned $CaCO_3$ through template-assisted MICP

To test whether the spatial distribution of MICP can be controlled through a template consisting of $CaCO_3$ precipitates, we first patterned the bottom glass surface of a Petri dish using colloidal suspensions consisting of precipitates collected from MICP process (Fig. 1(a), see Methods and ESI† for more details). After the pattern had been air-dried and UV-sterilized, fresh liquid culture of *S. pasteurii* containing urea was filled into the dish. As bacterial cells grew and multiplied, MICP process was continued, during which urea was hydrolyzed by urease produced by cells to generate ammonium and carbonate ions, which led to an increased pH in the local environment. The rise in pH then induced the precipitation of $CaCO_3$ in the presence

of Ca^{2+}. After 48 h-incubation, a clear pattern having the same shape as the template but with a more solid and bolded appearance formed. Fig. 1(b) shows a disk pattern from a disk template. Different spatial patterns can also be obtained using different designed templates (see one example in Fig. S1†). A quantitative measurement of the surface density of $CaCO_3$ precipitates, ρ_s, along the radial direction shows that ρ_s is over five times higher at the template region than at the template-free region (Fig. 1(c)), implying that there is much more accumulation of precipitates over the template than other places. This preferred precipitation at the template region also causes ρ_s of the template-free region to be even lower than that when there is no template used in control samples under otherwise same conditions. Together, these results clearly demonstrate the successful control of the spatial distribution of MICP through a template-based approach.

$CaCO_3$ is the main component of the template responsible for the preferred MICP on template

The XPS measurement of precipitates used for making the template shows that besides Ca, C and O, N and P are also detected (Fig. 2(a)). Such elements are most likely from bacteria associated sources. To determine the main component of the template that is responsible for its promoting effect for MICP, we first checked the role of organic materials contained in precipitates. Using both pure heat-killed *S. pasteurii* cells and heat-treated MICP-induced $CaCO_3$ particles (to burn out the possible attached organic materials on particles, if they have) as template materials, we repeated the above experiments of MICP
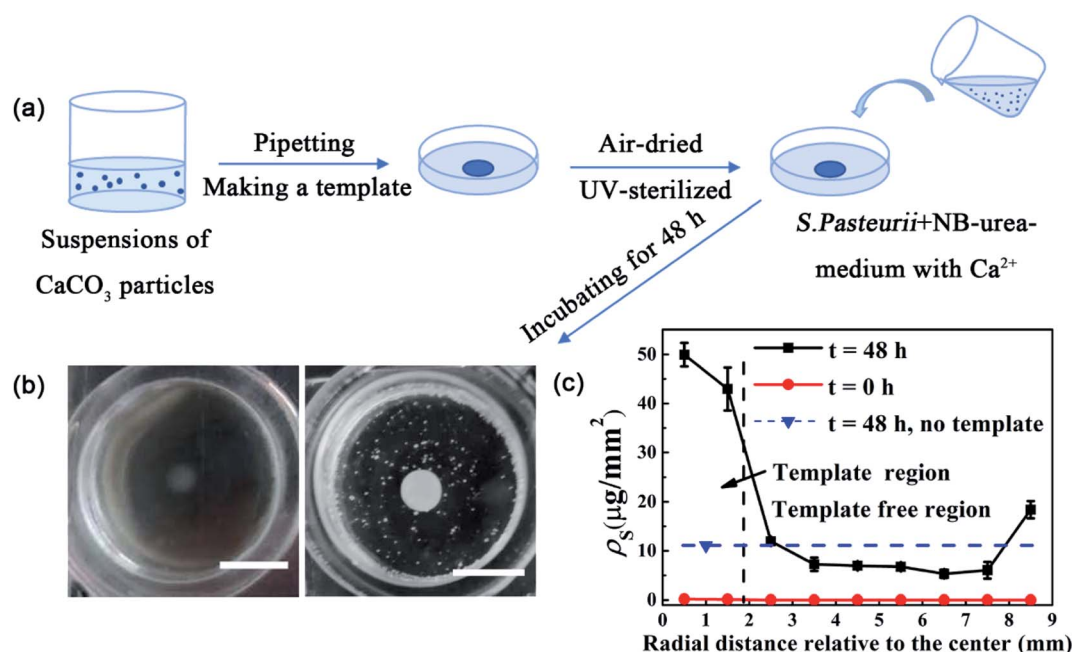

Fig. 1 Schematic illustration of the fabrication of patterned MICP through a template-based approach. (a) Scheme of the approach. (b) Photographs of a templated (disk-shape) glass surface at $t = 0$ h and $t = 48$ h after incubated in bacterial culture. The disk-shaped template is made of a suspension of MICP-induced $CaCO_3$ particles with a concentration of 1.5 mg mL^{-1}. Scale bars are 6 mm. (c) The surface density of $CaCO_3$ precipitates, ρ_s, along the radial direction. The rise at the largest radius is likely due to the boundary effect of container walls. Error bars show the standard deviations from three repeats.
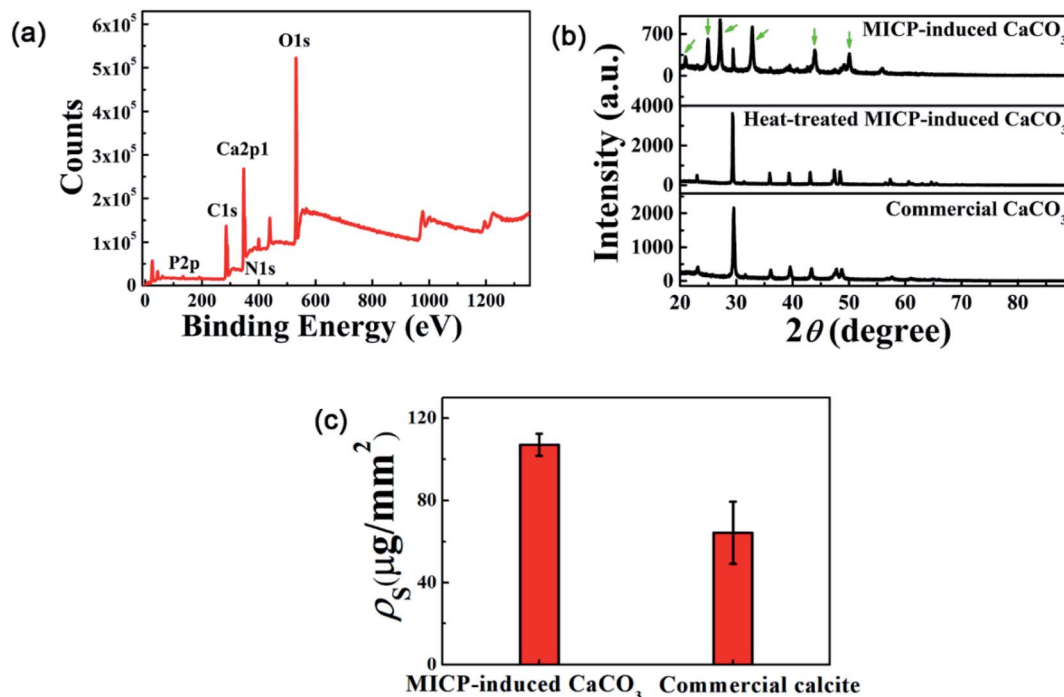
Fig. 2 Characterization of MICP precipitates. (a) XPS measurement of MICP-induced CaCO₃ particles. (b) XRD measurements of three types of CaCO₃ particles used in the study, including MICP-induced (green arrows point to characteristic peaks of vaterite, and the other peaks are for calcite), heat-treated MICP-induced, and commercial CaCO₃ particles. (c) ρ_s after 48 h incubation. Error bars show the standard deviations from three repeats.

precipitation on templated glass surfaces. The results show a preferred deposition of MICP at the template region for the latter case but not for the former case (Fig. S2(a), (e), (c) and (g)†), which excludes the possibility of the organic material contained in the template to be the main factor for the resulted preferential deposition of MICP. To see whether the negative-charged surface can lead to such phenomena, sulfonic group modified polystyrene (PS) particles having negative-charged surfaces, were also tested as a template, and no preferential deposition of MICP was observed (Fig. S2(b) and (f)†). This result agrees with observations in an earlier report.[29] Next, we used commercial CaCO₃ particles to make a template, and the preferred growth of precipitates at the template region was again observed (Fig. S2(d) and (h)†). Taken together, these results show that CaCO₃ of the template is the key ingredient responsible for the preferred deposition of MICP at the template region.

CaCO₃ has three different types of crystal structures, which are vaterite, calcite and aragonite.[30] The XRD measurements of the MICP-induced CaCO₃ particles show characteristic peaks of both calcite and vaterite with higher intensity peaks of vaterite than calcite (green arrows in Fig. 2(b)), indicating that MICP-induced CaCO₃ particles used in this study are mostly vaterite but also contain a less amount of calcite. By contrast, heat-treated MICP-induced CaCO₃ particles, show only peaks of calcite, same as commercial CaCO₃ particles do (Fig. 2(b)). This result consists with a previous report that vaterite is not stable and easily transformed into calcite at high temperature.[31] Interestingly, by making two templates side by side on the same

glass surface, which are made of MICP-induced and commercial CaCO₃ particles, respectively, the results show that the pattern formed at the former template region is much denser and clearer than that at the latter one (Fig. S3†), indicating that vaterite may have a stronger promoting effect for the deposition of MICP than calcite does. Such difference in the promoting effect of template can be seen more clearly from ρ_s measurements, which show that ρ_s of the template of MICP-induced CaCO₃ particles is about 1.7 times as big as that of the one formed by commercial CaCO₃ particles (Fig. 2(c) and S4†). In the following text, if not specified otherwise, the template is made of MICP-induced CaCO₃ particles.

Parameter optimization

To improve the promoting efficiency of template for MICP, several parameters including the concentration of calcium ions $C_{Ca^{2+}}$, incubation temperature T_i, as well as the properties of template,[27,28] were optimized. The results are shown in Fig. 3. We can see that ρ_s first increases with $C_{Ca^{2+}}$ and then reaches a plateau when $C_{Ca^{2+}} > 80$ mM under our conditions (Fig. 3(a)). MICP process is highly influenced by cultural temperature, and lowing temperature would decrease the urease activities,[23] which has also been confirmed in this study (Fig. S5†). However, under our conditions, we find that ρ_s first increases as T_i decreases from 30 °C to 15 °C and then decreases as T_i continues to drop down to 10 °C (Fig. 3(b), also see Fig. S6† for typical images obtained at different T_i). Since the template acts as growth sites for MICP process, ρ_s will also depend on the
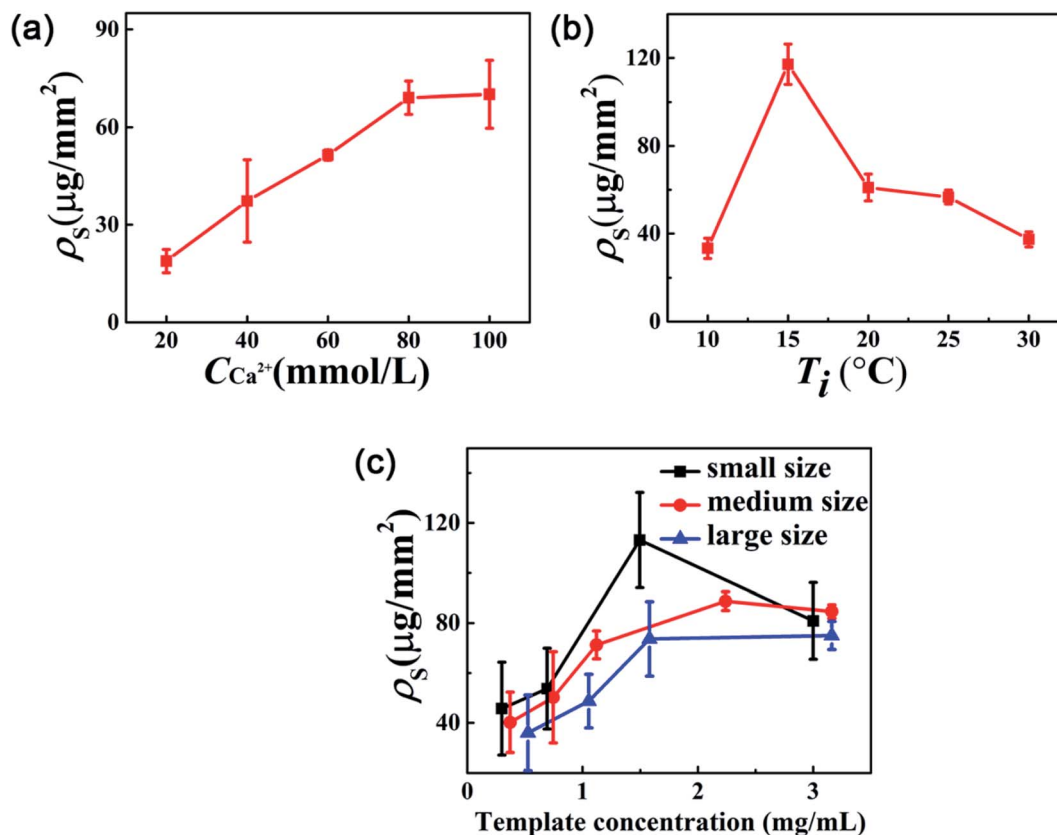
Fig. 3 Optimization of the fabrication parameters. Template promoting efficiency changes with (a) Ca^{2+} concentration (with small-sized $CaCO_3$ particles), (b) cultural temperature (with small-sized $CaCO_3$ particles), and (c) template concentration for different sized $CaCO_3$ particles. Error bars show the standard deviations from three repeats.

properties of template. Fig. 3(c) shows the measured ρ_s *vs.* the template concentration (*i.e.*, the mass concentration of $CaCO_3$ particles used to make templates) at 15 °C. Three different sized MICP-induced $CaCO_3$ particles were tested, which have a size distribution peaked at ~1 μm (small-size), 4.5 μm (medium-size), and 6 μm (large-size) (Fig. S7†), respectively. From the figure, we can see that for each sized $CaCO_3$ particles, ρ_s first increases relatively rapidly with the template concentration and then changes gradually when the concentration is higher than 1.5 mg mL^{-1}. Moreover, by comparing the ρ_s of the small-size (ρ_s^{small}), medium-size (ρ_s^{medium}), and large-size (ρ_s^{large}) $CaCO_3$ particles, we can see that before 1.5 mg mL^{-1}, ρ_s at the same mass concentration of $CaCO_3$ particles shows a trend of $\rho_s^{small} > \rho_s^{medium} > \rho_s^{large}$, *i.e.*, ρ_s decreases with the size of $CaCO_3$ particles. The observed dependence of ρ_s on the template concentration can be understood in terms of the exposed surface areas of $CaCO_3$ particles. When the template concentration increases from a very dilute value, the total exposed surface area of $CaCO_3$ particles in the template also increases, *i.e.*, there are more available growth sites, which then leads to a higher promoting efficiency of the template. But after the template concentration reaches to a value (about 1.5 mg mL^{-1} under our conditions) where the whole template region is fully covered by a monolayer of $CaCO_3$ particles, the total exposed surface area of $CaCO_3$ particles would be saturated, and thus the deposition density roughly reaches a plateau. Similarly,

one may also imagine that by reducing the size of $CaCO_3$ particles, the total exposed surface area of these particles can also be increased given the same total mass of particles, therefore, ρ_s would increase when smaller sized $CaCO_3$ particles are used, which are exactly what we observed in the experiments.

By employing these optimized conditions, *i.e.*, when $C_{Ca^{2+}} = 80$ mM, $T_i = 15$ °C, and using the template made of small-sized $CaCO_3$ particles with a concentration of 1.5 mg mL^{-1}, better patterns were obtained (Fig. 4), which display more sharpen edges and have higher contrast with the non-template region than the pattern shown in Fig. 1 (or Fig. S1†) which was formed under non-optimized conditions. Moreover, by employing a template array of disks, a periodic patterned $CaCO_3$ materials was successfully fabricated (see one example of 4 × 4 array in Fig. 4), indicating the scalability of this method in fabricating large-scale $CaCO_3$ materials with controlled spatial arrangement.

Discussion

For successfully patterned MICP precipitation at the template region, it is ideal to have promoted heterogeneous nucleation and growth at the template region but suppressed homogeneous nucleation in solution. According to classical crystallization theories,[32–34] the free energy for formation of stable nuclei (ΔG) at an interface can be expressed as
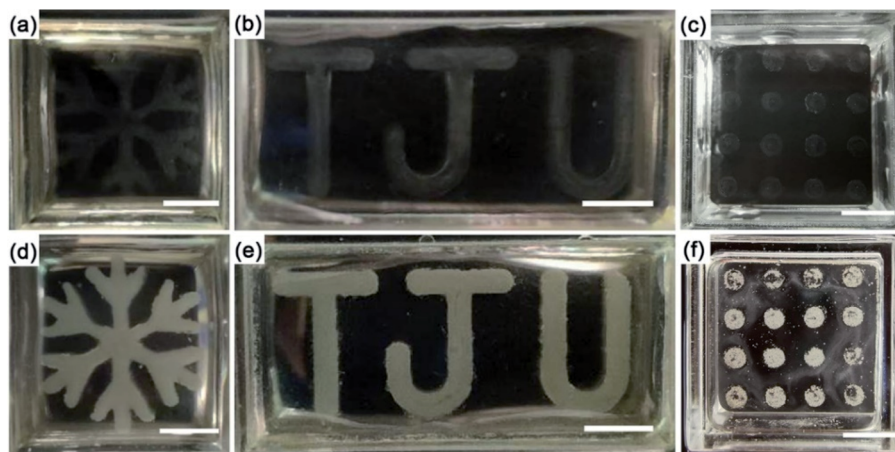
Fig. 4 MICP precipitates with different patterns obtained under optimized conditions. (a–c) At $t = 0$ h, and (d–f) at $t = 48$ h. Scale bars are 6 mm.

$$\Delta G = -RT \ln S + \sigma_{cl} A_{cl} + (\sigma_{cs} - \sigma_{sl}) A_{cs} \quad (1)$$

where, R is the ideal gas constant, T is the temperature, S is the degree of supersaturation, σ is the interfacial energy, A is the particle surface area. The subscripts c, l, s refer to crystalline particle, the liquid phase and the substrate, respectively. It has been shown that the template can greatly promote heterogenous nucleation by having a lower net interfacial energy than particle-solution interfacial energy, and thus under the same supersaturation conditions, the nucleus formed by heterogenous nucleation can be about one order of magnitude bigger than that formed by homogenous one.[34] In this work, by using the MICP precipitates as the template material, the net interfacial energy is lowered not only when compared with that of homogenous nucleation in solution, but also when compared with that of heterogeneous nucleation at other non-templated glass surface, as σ_{cs} is essentially zero when MICP precipitates used as the template material whereas σ_{cs} of glass and CaCO$_3$ is larger than zero. Thus the template region will show promoted precipitation.

During MICP process, it has been suggested that the less stable, amorphous calcium carbonate (ACC) nanoparticles are first formed and then crystallize into crystalline calcium carbonate polymorphs.[35–37] The interfacial energy between ACC and vaterite will be less than that between ACC and calcite since vaterite is less stable than calcite. This can explain why the promoting efficiency of MICP-induced precipitates (which are mainly vaterite) is higher than commercial ones (which are calcite).

In this work, we observed that the promoting efficiency of template for MICP is optimized at $T_i = 15$ °C within the tested temperature range of 10–30 °C. However, the bacterial growth curves show that bacteria grow faster and better as T_i increases (Fig. S5(a)†). Correspondingly, for bacterial cultures which start with a similar cell concentration, their urease activities also display a better performance at higher temperatures (Fig. S5(b)†). These results indicate that besides the urease activity of bacterial culture, there are also other temperature-associated factors that would contribute to the observed maximum ρ_s at $T_i = 15$ °C.

One such possible factor would be the diffusion of calcium and carbonate ions (*i.e.*, the influence of mass transport) during MICP. With the continuation of MICP precipitation at the template region, calcium and carbonate ions over this region would be depleted to the point of undersaturation, which can then be supplemented by the diffusion of ions from nearby regions under no flow conditions. Thus, by tuning the relative ratio of the consuming rate and the diffusion rate of calcium and carbonate ions over the template region through temperature (as these two rates are both affected by temperature), the efficiency of the template can be controlled. Specifically, in our case, what we think have happened is the following. At high $T_i = 30$ °C, the urease activity is strong and induces a high concentration of carbonate ions, which changes the tested bacterial solution quickly into a supersaturated state for CaCO$_3$. Although the precipitation in the template region starts relatively easily due to the lower net interfacial energy for the nucleation of precipitates on CaCO$_3$ particles, the rapid supersaturation in the non-template region can also induce the precipitation of CaCO$_3$. As a consequence, the precipitation will happen not only in the template region but also in the non-template region, thus the precipitated CaCO$_3$ in the template region is reduced (under the same total amount of calcium ions). When T_i decreases from 30 °C to 15 °C, the urease activity goes down (Fig. S5(b)†) so the concentration of carbonate ions increases but slowly. As soon as the concentration of carbonate ions reaches to a certain level, the preferred precipitation in the template region would happen, which then will deplete the concentration of calcium and carbonate ions to the point of undersaturation in the template region and cause a concentration gradient to drive the diffusion of ions from nearby regions to the template region. Because the consuming rate of calcium and carbonate ions would be slowed down as T_i decreases, the diffusion of ions from nearby regions could be relatively easily to maintain the level of calcium and carbonate ions and keep the preferred precipitation continuing over the template region, thus the promoting efficiency is increased. But when T_i continues to drop down to 10 °C, the urease activity is reduced so much (Fig. S5(b)†) that the solution is deficient in the amount of carbonate ions and thus result in a large decrease in MICP. This diffusion-controlled process is similar to that

observed using SAM template.[8] This hypothesis is also consistent with the observation that there are more $CaCO_3$ precipitates in the non-templated region as T_i increases (Fig. S6†), but to quantitatively determine the relationship between T_i and the template efficiency for MICP needs further studies. In addition, as bacterial growth is temperature-dependent, it would be also interesting to see how the bacterial concentration affects the observed temperature-dependent promoting efficiency of template in future studies.

Conclusion

In summary, as a proof of concept, this work demonstrated a simple and efficient way to control the spatial distribution of MICP-induced $CaCO_3$ precipitates with essentially arbitrary 2D patterns through a template-assisted approach. Parameters like $C_{Ca^{2+}}$, T_i, the concentration and size of $CaCO_3$ particles used in templates were optimized, under which patterns with much better quality were obtained. Compared with traditional ceramic processing routes, this method is green, environmentally friendly, scale-upable and is also conducted under mild conditions, and thus has a great potential for applications in fabricating patterned calcium carbonate materials.

Methods

Bacterial strain and growth conditions

Bacteria *S. pasteurii* (ATCC 11859) was used in this study. Bacterial cells were cultured in YE-urea liquid medium (2% w/v urea, and YE for yeast extract 20 g L^{-1}, ammonium sulfate 10 g L^{-1}, Tris 0.13 M) at 30 °C, 220 rpm (rotations per minute) or on YE-urea plates containing 2% agar. MICP experiments were carried out in nutrient broth (NB)-urea medium (2% w/v urea, and NB for peptone 10 g L^{-1}, beef extract 10 g L^{-1}, NaCl 5 g L^{-1}, ammonium sulfate 10 g L^{-1}). Urea solution and $CaCl_2 \cdot 2H_2O$ solution were filter-sterilized through 0.22 μm pore size filters and added later. All other media components were autoclaved separately at 121 °C for 15 min and mixed together before inoculation. Heat-killed *S. pasteurii* cells were obtained by autoclaving cell suspensions for 30 min at 121 °C.

Collecting $CaCO_3$ precipitates produced by MICP process

S. pasteurii cultures were grown overnight at 30 °C in YE-urea medium to an optical density at 600 nm (OD_{600}) ∼1.6. Then cells were harvested by centrifugation at ∼2000 g for 5 min, and resuspended in NB-urea medium (Ca-free). Next, the resuspended bacteria were diluted in 100 mL NB-urea medium containing 25 mM $CaCl_2$ to a final OD_{600} of 0.02, and were incubated on an orbital shaker at 30 °C for 10 h. After 10 h-incubation, precipitates were collected by centrifugation, which were then subject to ultrasonication and washed for three times using deionized (DI) water to remove attached bacteria cells. The cleaned $CaCO_3$ precipitates were dried at 60 °C for 24 h and then were ready for further use. The heat-treated MICP $CaCO_3$ particles were obtained by furnacing the above collected MICP $CaCO_3$ particles in a Muffle furnace (JXR1200-30, Shanghai Junke Instrument Technology Co., Ltd) at 450 °C for 3 h (Table S1†).

Template-assisted MICP

To make a template on a glass surface, a suspension of each specific material was first formed either by dispersing dried solid particles into water to the target concentration for MICP-induced, heat-treated MICP-induced, commercial $CaCO_3$ particles and sulfonic group modified PS particles, or by diluting the heat-killed *S. pasteurii* culture using NB-urea medium to an OD_{600} of ∼1. Next, to make a single disk-shaped template, a 2 μL drop of the suspension was pipetted onto the glass surface of a 18 mm glass-bottom Petri dish, which was then air-dried and treated with ultraviolet (UV) light. Other shaped templates were fabricated either by directly hand-drawing a pattern using a pipet or through an acrylic pattern obtained by laser-cutting (Yueming Laser, CMA6040). When an acrylic plate with a cut-out pattern was used to make a template, agar gel (1.5% w/v) was used to seal the gap between the acrylic plate and the glass first before the addition of $CaCO_3$ particle suspension, and once the added suspension dried, both the acrylic plate and the agar gel were removed to leave dried template only on the glass surface. Then a squared fence made of acrylic was glued onto the glass, which enclosed the template region to form a square well (with a size of 18 mm × 18 mm × 5 mm). Subsequently, the dish/square well was filled gently with 470–1200 μL (depending on the template) of diluted bacterial suspension with an OD_{600} of 0.02 in NB-urea medium containing specified concentration of $CaCl_2$. Then the dish/square well was sealed using parafilm and left still in an incubator at 15 °C for 48 h. After the incubation, the dish/square well was then placed on an optical microscope for imaging.

For the optimization of parameters to improve the promoting efficiency of template for MICP, disk-shaped templates were used.

Microscopy and precipitation analysis

Images were captured using a sCMOS camera (Andor, Neo) on a Leica DMi8 inverted optical microscope with a 10× objective. XRD measurements were performed using a D8 Focus X-ray diffractometer (Bruker) in the diffraction angle range $2\theta = 20$–$90°$, using Cu Kα radiation (40 kV and 40 mA). XPS measurements were conducted using an X-ray photoelectron spectroscopy (XPS, Thermo Fisher Scientific) with an Al Kα (150 eV) X-ray.

The surface density of precipitates ρ_s is determined as the following: after a specified period of incubation, *e.g.*, 48 h, the Petri dish with the patterned glass bottom was washed gently for three times using DI water and then dried at 60 °C in an oven. For a typical measurement of ρ_s of the template region, the total mass of the dish with the dried MICP pattern on the glass bottom was first weighted to be m_1; next, the precipitates at the template region were removed using a tweezer; after that, the whole dish was weighted again to get m_2, then the mass of precipitates was obtained by $m_1 - m_2$. ρ_s is obtained by dividing $m_1 - m_2$ with the area of template region. We note that the mass of initial deposited precipitates used as the template is at least one order of magnitude smaller than that of final precipitates at the template region, and thus is neglected.

For measuring ρ_s along the radius direction of the Petri dish as shown in Fig. 1, we first split the round Petri dish area in the photo to 9 concentric annuli (Fig. S8†). Then, for each annular zone in the template region, ρ_s is calculated as described above. However, for each annular zone in the template free region, since the total mass of the precipitates in such zones is too small to be weighted accurately under our conditions, it was estimated by the sum of the mass of each precipitated particle in the zone. The mass of each particle is estimated as the product of $CaCO_3$ density and the volume of the particle, which is assumed to be spherical and its diameter is measured by ImageJ.

Urease activity measurement

Urease activity was determined by a conductivity method in the absence of calcium ions.[38–40] 1 mL of bacterial culture was added into 9 mL of 1.1 mol L^{-1} urea solution, whose conductivity was then monitored for 5 min by a conductivity meter. The urease activity of the ureolytic bacteria can be calculated by multiplying the averaged variation rate of conductivity within 5 min (ms cm^{-1} min^{-1}) with the dilution factor (10 times) and 11.11, i.e., the hydrolysis rate of urea (mmol L^{-1} min^{-1}) = the variation rate of conductivity (ms cm^{-1} min^{-1}) × 11.11.

Author contributions

K. Z. conceived and designed the project. D. Y. and H. Z. performed experimental measurements. D. Y., H. Z., W. Z. and Y. Z. analyzed data. D. Y., H. Z. and K. Z. wrote the paper. All authors discussed the results and commented on the manuscript.

Conflicts of interest

There are no conflicts to declare.

Acknowledgements

References

1 H. A. Lowenstam and S. Weiner, *On Biomineralization*, Oxford University Press, New York, U.K., 1989.

2 D. Walsh and S. Mann, Fabrication of hollow porous shells of calcium carbonate from self-organizing media, *Nature*, 1995, **377**, 320–323.

3 D. C. Popescu, E. N. M. V. Leeuwen, N. A. A. Rossi, *et al.*, Shaping Amorphous Calcium Carbonate Films into 2D Model Substrates for Bone Cell Culture, *Angew. Chem.*, 2006, **118**, 1794.

4 S. Mann, B. R. Heywood, S. Rajam, *et al.*, Controlled crystallization of $CaCO_3$ under stearic acid monolayers, *Nature*, 1988, **334**, 692–695.

5 G. Xu, N. Yao, I. A. Aksay, *et al.*, Biomimetic Synthesis of Macroscopic-Scale Calcium Carbonate Thin Films. Evidence for a Multistep Assembly Process, *J. Am. Chem. Soc.*, 1998, **120**, 11977.

6 E. Loste, E. Díaz-Martí, A. Zarbakhsh, *et al.*, Study of Calcium Carbonate Precipitation under a Series of Fatty Acid Langmuir Monolayers Using Brewster Angle Microscopy, *Langmuir*, 2003, **19**, 2830–2837.

7 A. Kumar, N. L. Abbott, H. A. Biebuyck, *et al.*, Patterned Self-Assembled Monolayers and Meso-Scale Phenomena, *Acc. Chem. Res.*, 1995, **28**, 219–226.

8 J. Aizenberg, A. J. Black and G. M. Whitesides, Control of crystal nucleation by patterned self-assembled monolayers, *Nature*, 1999, **398**, 495–498.

9 J. Aizenberg, Direct Fabrication of Large Micropatterned Single Crystals, *Science*, 2003, **299**, 1205–1208.

10 A. M. Travaille, L. Kaptijn, P. Verwer, *et al.*, Highly oriented self-assembled monolayers as templates for epitaxial calcite growth, *J. Am. Chem. Soc.*, 2003, **125**, 11571.

11 I. Lee, S. W. Han, S. J. Lee, *et al.*, Formation of Patterned Continuous Calcium Carbonate Films on Self-Assembled Monolayers via Nanoparticle-Directed Crystallization, *Adv. Mater.*, 2002, **14**, 1640–1643.

12 C. Lu, L. Qi, J. Ma, *et al.*, Controlled Growth of Micropatterned, Oriented Calcite Films on a Self-Assembled Multilayer Film, *Langmuir*, 2004, **20**, 7378–7380.

13 T. Zhu and M. Dittrich, Carbonate Precipitation through Microbial Activities in Natural environment, and Their Potential in Biotechnology: A Review, *Front. Bioeng. Biotechnol.*, 2016, **4**, 588.

14 W. De Muynck, N. De Belie and W. Verstraete, Microbial carbonate precipitation in construction materials: a review, *Ecol. Eng.*, 2010, **36**, 118–136.

15 A. Vahabi, A. A. Ramezanianpour, H. Sharafi, *et al.*, Calcium carbonate precipitation by strain Bacillus licheniformis AK01, newly isolated from loamy soil: a promising alternative for sealing cement-based materials, *J. Basic Microbiol.*, 2015, **55**, 105–111.

16 Q. Li, L. Csetenyi and G. M. Gadd, Biomineralization of Metal Carbonates by Neurospora crassa, *Environ. Sci. Technol.*, 2014, **48**, 14409–14416.

17 A. Liang, C. Paulo, Y. Zhu, *et al.*, $CaCO_3$ biomineralization on cyanobacterial surfaces: insights from experiments with three Synechococcus strains, *Colloids Surf., B*, 2013, **111**, 600–608.

18 C. M. Kirkland, S. Zanetti, E. Grunewald, *et al.*, Detecting Microbially Induced Calcite Precipitation in a Model Well-Bore Using Downhole Low-Field NMR, *Environ. Sci. Technol.*, 2017, **51**, 1537–1543.

19 D. Martin, K. Dodds, B. T. Ngwenya, *et al.*, Inhibition of Sporosarcina pasteurii under Anoxic Conditions: Implications for Subsurface Carbonate Precipitation and Remediation via Ureolysis, *Environ. Sci. Technol.*, 2012, **46**, 8351–8355.

20 V. P. Pham, A. Nakano, d. S. Van, *et al.*, Applying MICP by denitrification in soils: a process analysis, *Environ. Geotech.*, 2016, **5**, 1–15.

21 F. Hammes and W. Verstraete, Key roles of ph and calcium metabolism in microbial carbonate precipitation, *Rev. Environ. Sci. Biotechnol.*, 2002, **1**, 3–7.

22 J. Peng and Z. Liu, Influence of temperature on microbially induced calcium carbonate precipitation for soil treatment, *PLoS One*, 2019, **14**, e0218396.

23 X. Sun, L. Miao, T. Tong, *et al.*, Study of the effect of temperature on microbially induced carbonate precipitation, *Acta Geotech.*, 2018, **14**, 627.

24 P. Anbu, C.-H. Kang, Y.-J. Shin, *et al.*, Formations of calcium carbonate minerals by bacteria and its multiple applications, *SpringerPlus*, 2016, **5**, 250.

25 G. D. O. Okwadha and J. Li, Optimum conditions for microbial carbonate precipitation, *Chemosphere*, 2010, **81**, 1143–1148.

26 W. D. Muynck, N. D. Belie and W. Verstraete, Microbial carbonate precipitation in construction materials: a review, *Ecol. Eng.*, 2010, **36**, 118–136.

27 W. Qin, C. Y. Wang, Y. X. Ma, *et al.*, Microbe-Mediated Extracellular and Intracellular Mineralization: Environmental, Industrial, and Biotechnological Applications, *Adv. Mater.*, 2020, **32**, 1907833.

28 N. Li, L. N. Niu, Y. P. Qi, *et al.*, Subtleties of biomineralisation revealed by manipulation of the eggshell membrane, *Biomaterials*, 2011, **32**, 8743–8752.

29 W. Zhang, Y. Ju, Y. Zong, *et al.*, In Situ Real-Time Study on Dynamics of Microbially Induced Calcium Carbonate Precipitation at a Single-Cell Level, *Environ. Sci. Technol.*, 2018, **52**, 9266–9276.

30 S. Mann, *Biomineralization: Principles and Concepts in Bioinorganic Materials Chemistry*, Oxford University Press, New York, U.K., 2001.

31 C. Rodriguez-Navarro, C. Jimenez-Lopez, A. Rodriguez-Navarro, *et al.*, Bacterially mediated mineralization of vaterite, *Geochim. Cosmochim. Acta*, 2007, **71**, 1197–1213.

32 R. Mohanty, S. Bhandarkar and J. Estrin, Kinetics of Nucleation from Aqueous Solution, *AIChE J.*, 1990, **36**, 1536–1544.

33 P. P. Chiang and M. D. Donohue, A kinetic approach to crystallization from ionic solution I. Crystal growth, *J. Colloid Interface Sci.*, 1988, **122**, 230–250.

34 B. C. Bunker, P. C. Rieke, B. J. Tarasevich, *et al.*, Ceramic Thin-Film Formation on Functionalized Interfaces Through Biomimetic Processing, *Science*, 1994, **264**, 48–55.

35 E. M. Pouget, P. H. H. Bomans, J. A. C. M. Goos, *et al.*, The Initial Stages of Template-Controlled CaCO₃ Formation Revealed by Cryo-TEM, *Science*, 2009, **323**, 1455–1458.

36 B. P. Pichon, P. H. H. Bomans, P. M. Frederik, *et al.*, A quasi-time-resolved CryoTEM study of the nucleation of CaCO₃ under Langmuir monolayers, *J. Am. Chem. Soc.*, 2008, **130**, 4034–4040.

37 J. D. Rodriguez-Blanco, S. Shaw and L. G. Benning, The kinetics and mechanisms of amorphous calcium carbonate (ACC) crystallization to calcite, viavaterite, *Nanoscale*, 2011, **3**, 265–271.

38 A. I. Omoregie, G. Khoshdelnezamiha, N. Senian, *et al.*, Experimental optimisation of various cultural conditions on urease activity for isolated *Sporosarcina pasteurii* strains and evaluation of their biocement potentials, *Ecol. Eng.*, 2017, **109**, 65–75.

39 M. Li, X. H. Cheng, Z. Yang, *et al.*, Breeding High-yield Urease-producing *Sporosarcina pasteurii* Strain by NTG Mutation, *J. Agric. Sci. Technol.*, 2013, **15**, 130–134.

40 V. S. Whiffin, *Microbial CaCO₃ precipitation for the production of biocement*, PhD thesis, Murdoch Univ., Perth, Australia, 2004.